Additive Manufacturing Letters 6 (2023) 100144

Contents lists available at ScienceDirect

Additive Manufacturing Letters

journal homepage: www.elsevier.com/locate/addlet

Short Communication

Microstructure of an additively manufactured Ti-Ta-Al alloy using novel pre-alloyed powder feedstock material

C. Lauhoff[a,*], T. Arold[b], A. Bolender[b], M.W. Rackel[c], F. Pyczak[c], M. Weinmann[d], W. Xu[a], A. Molotnikov[a], T. Niendorf[b]

[a] RMIT Centre for Additive Manufacturing, School of Engineering, RMIT University, Melbourne, VIC, 3000, Australia
[b] Institute of Materials Engineering, University of Kassel, Mönchebergstr. 3, 34125, Kassel, Germany
[c] Helmholtz-Zentrum Hereon, Max-Planck-Str. 1, 21502, Geesthacht, Germany
[d] TANIOBIS GmbH, Im Schleeke 78 – 91, 38642, Goslar, Germany

ARTICLE INFO

Keywords:
PBF-EB/M
Alloy formation
EIGA
Chemical homogeneity
Refractory metals
Synchrotron diffraction

ABSTRACT

Binary Ti-Ta and ternary Ti-Ta-Al alloys attracted considerable attention as new potential biomaterials and/or high-temperature shape memory alloys. However, conventional forming and manufacturing technologies of refractory based titanium alloys are difficult and cost-intensive, especially when complex shapes are required. Recently, additive manufacturing (AM) emerged as a suitable alternative and several studies exploited elemental powder mixing approaches to obtain a desired alloy and subsequently use it for complex shape manufacture. However, this approach has one major limitation associated with material inhomogeneities after fabrication. In present work, novel pre-alloyed powder material of a Ti-Ta-Al alloy was additively manufactured. Hereto, electron beam powder bed fusion (PBF-EB/M) technique was used for the first time to process such Ti-Ta based alloy system. Detailed microstructural analysis revealed that additively manufactured structures had a near full density and high chemical homogeneity. Thus, AM of pre-alloyed feedstock material offers great potential to overcome major roadblocks, even when significant differences in the melting points and densities of the constituents are present as proven in the present case study. The homogeneous microstructure allows to apply short-term thermal post treatments. The highly efficient process chain detailed will open up novel application fields for Ti-Ta based alloys.

1. Introduction

Nowadays, additive manufacturing (AM) techniques are widely adopted in academia and industry to fabricate functional metal parts and components of unprecedented geometrical complexity. For the two major categories of metal AM technologies, i.e. powder bed fusion (PBF) and directed energy deposition (DED), structures are fabricated directly from a computer-aided design (CAD) file through layer wise melting of either powder or wire feedstock material. The possibility for a tool-free design allows to overcome limitations of conventional manufacturing processes, especially when challenging materials have to be processed causing high production costs [1]. Furthermore, AM techniques were reported to be employed for direct microstructure design. By controlling the thermal gradient and the solidification velocity via an adequate choice of the processing parameters, local microstructural features and, thus, mechanical properties can be tailored [2–5]. Given these AM characteristics, topology optimized geometries and locally tailored microstructures can lead to a new generation of lightweight designs being highly attractive for applications in the automotive, aerospace and biomedical sectors.

Over the last two decades, a variety of materials were qualified for AM technologies to open up new industrial markets [6,7]. Among these materials, titanium and its alloys are particularly prominent due to their superior properties, i.e. high strength to weight ratio, good biocompatibility, and excellent corrosion resistance [8]. Ti-Ta alloys have attracted significant attention for multipurpose use as bone implants as well as high-temperature actuators due to an enhanced osseointegration [9–11] and shape memory properties [12], respectively.

Binary Ti-Ta alloys compete with Ti-6Al-4V, the latter being the most common alloy used for orthopedic implants. Tremendous efforts have been devoted on processing of Ti-6Al-4V via AM and the relationships between process, microstructure and mechanical properties are well understood [13–15]. However, the suitability of Ti-6Al-4V as bone implant alloy has recently been questioned due to potential toxicity concerns associated with the alloying elements [16,17] and its inherently high elastic modulus of 113 GPa being much higher than that of human bone (5 –

* Corresponding author.
E-mail address: christian.lauhoff@rmit.edu.au (C. Lauhoff).

https://doi.org/10.1016/j.addlet.2023.100144
Received 23 March 2023; Received in revised form 21 April 2023; Accepted 1 May 2023

30 GPa). The latter promotes the stress-shielding effect, bone resorption and eventually implant failure [18]. Alloying titanium with tantalum, in turn, seems to be a highly promising approach for designing novel biomaterials. Tantalum is known for its nontoxic nature and Ti-Ta alloys were reported to show reduced elastic moduli [19], leading to better biocompatibility and superior implant integration with the human body (compared to Ti-6Al-4V [9–11]), respectively.

Furthermore, Ti-Ta alloys can feature shape memory behavior well above 100°C and, thus, came into focus of research as high-temperature shape memory alloy (HT-SMA) candidates [12,20]. Their unique functional properties are based on a thermoelastic, reversible phase transformation between the high-temperature austenitic β-phase (body-centered cubic, bcc) and the low-temperature martensitic α''-phase (orthorhombic) [12]. Transformation strains of up to 3.6% were reported [21]. Unfortunately, binary Ti-Ta is prone to rapid functional degradation during thermal or thermo-mechanical cycling. Formation of the hexagonal ω-phase leads to the stabilization of the high-temperature β-phase, resulting in a deterioration or even loss of the functional properties [12,22,23]. However, alloying with ternary elements such as tin and aluminum can improve the functional stability by delaying the formation of the ω-phase [21,24,25]. In addition, compared with Ni-Ti-Hf, being currently the most promising HT-SMA system [26,27], Ti-Ta-*X* (e.g. *X* = Al, Sn) HT-SMAs contain more reasonably priced constituents and provide good workability [12,25].

Despite these advantages, Ti-Ta(-Al) alloys are still not widely adopted in industrial applications. The challenging alloy formation caused by the substantial differences in the alloying elements' melting points and densities is a major roadblock towards their widespread use. The differences can cause vaporization of the lower-melting elements and chemical inhomogeneities by segregation of the constituents during the solidification process, respectively [28,29]. In case of conventional processing, alloy ingots must be remelted and annealed many times to obtain adequate homogeneity [28]. Recently, AM came into focus as a new processing route being capable to produce refractory titanium alloys (e.g. Ti-Nb, Ti-Ta) via *in situ* alloying. Since in most cases pre-alloyed feedstock material was not available so far, it was shown that mechanical mixing of elemental powders and subsequent processing can lead to the desired alloy fabrication [30–35]. However, it was noted that *in situ* alloying results in local inhomogeneity of the microstructure due to presence of unmolten niobium and tantalum particles, at least when the energy input is too low. On the other hand, an increase in energy leads to substantial keyhole formation [30–32]. Some success was reported by Brodie et al. [32–34] for Ti-Ta and Huang et al. [35] for Ti-Nb. To promote homogeneity, the authors utilized a remelting scanning strategy. However, this approach reduces the productivity of the AM process and limits its applicability of printing structures with fine features.

Pre-alloyed feedstock material is an optimal candidate to overcome aforementioned limitations. One example was reported by Schulze et al. [36] focusing on a Ti-Nb alloy. Ternary Ti-Nb-Ta pre-alloyed powders especially designed for application in AM processes have been recently patented [37]. However, to the best of the authors' knowledge, no work has been published on AM of pre-alloyed Ti-Ta based material. Furthermore, all of the previous studies about additively manufactured Ti-Ta based alloy systems focused on laser beam powder bed fusion (PBF-LB/M, abbreviation according to ISO/ASTM 52900 standard terminology). Thus, in order to close this prevailing gap, the present study reports on a pre-alloyed Al-modified Ti-Ta alloy and its processing by electron beam powder bed fusion (PBF-EB/M). Aim of the investigations conducted was to shed light on the microstructural evolution along the whole process chain from feedstock material to additively manufactured bulk material. Hereto, detailed microstructure analysis has been performed using optical and scanning electron microscopy as well as high-energy synchrotron diffraction. In particular, alloy formation being characterized by a homogenous element distribution is proven for this highly challenging processing conditions, i.e. processing under vacuum of an alloy system featuring melting point and density differences in extreme.

Table 1
PBF-EB/M processing parameters used for fabrication of the Ti-Ta-Al samples investigated in the present study.

Heating before process start	
Start temperature	850 °C
Hold time before process start	1200 s
Preheating	
Beam speed	12000 mm/s
Beam current	18 mA
Focus offset	75 mA
Number of repetitions	9
Melting	
Acceleration voltage	60 kV
Beam speed	3500 mm/s
Beam current	10 mA
Focus offset	3 mA
Hatch distance	0.1 mm
Layer thickness	0.05 mm

2. Material and methods

2.1. Material and processing

In the present study, a Ti-Ta-Al alloy with a nominal chemical composition of Ti-25Ta-5Al (wt.-%) was additively manufactured. While a tantalum content of 25 wt.-% was chosen in light of orthopedic implant applications [10,19], small amounts of Al have been added (regardless of the potential toxicity concerns for biomaterials) due to its well-known stabilizing effect on shape memory properties [21,24]. Thereby, an alloy system with constituents featuring highly different physical properties was evaluated. Pre-alloyed powder feedstock material was produced via electrode induction melting inert gas atomization (EIGA). For powder manufacturing, pure elemental powders were blended and subsequently cold isothermally pressed (CIP) to form rod-shaped electrode material with a diameter of 45 mm and a length of about 330 mm. Employing a Leco TC-436 analysing unit, the oxygen and nitrogen contents of the CIP rod were determined to be 2834 µg/g and 292 µg/g, respectively. The carbon content was found to be 120 µg/g using a Leco TC-444 analyzing system. The atomization process was performed using inert argon gas (99.999%) at a gas pressure of 25 bar. From the obtained spherical powder, a powder fraction featuring nominal particle sizes between 63 and 125 µm was extracted by sieving.

The PBF-EB/M process was conducted on a GE Additive Arcam A2X machine. In order to limit the volume of required powder material, a build plate reduction with dimensions of 50 × 50 mm^2 was utilized. Cuboidal blocks with dimensions of 10 × 10 mm^2 base area and 50 mm in height were fabricated on a steel (AISI 304) build plate employing beam currents and beam speeds in a range of 7 – 13 mA and 2500 – 3500 mm/s, respectively. A bidirectional meander scanning strategy with 90° rotation between successive layers was employed. In each layer, the exposure was accomplished block by block. For the sake of brevity, only the material processed using the set of parameters leading to the highest density is detailed in the present paper. A summary of these processing parameters is given in Table 1. Using those values for the acceleration voltage, beam current, beam speed, and hatch distance, the resulting energy per unit area is calculated to be 1.71 J/mm^2.

2.2. Sample preparation and characterization

Plates of 1.5 mm thickness were machined along the build direction (BD) from the PBF-EB/M manufactured cuboids by electro-discharge

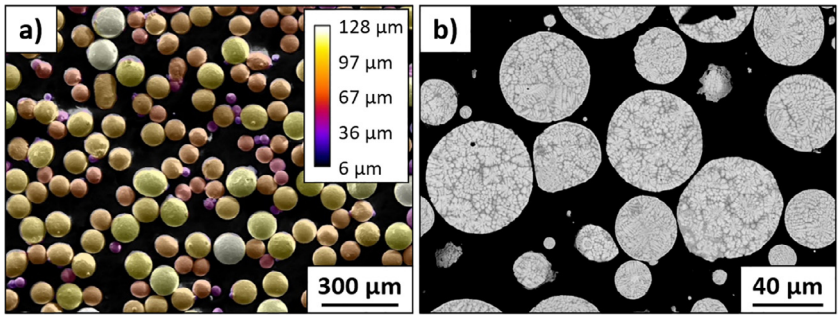

Fig. 1. SEM analysis of pre-alloyed Ti-Ta-Al powder material processed by EIGA: (a) SE image with superimposed color coding indicating the size of each powder particle and (b) cross-section BSE image.

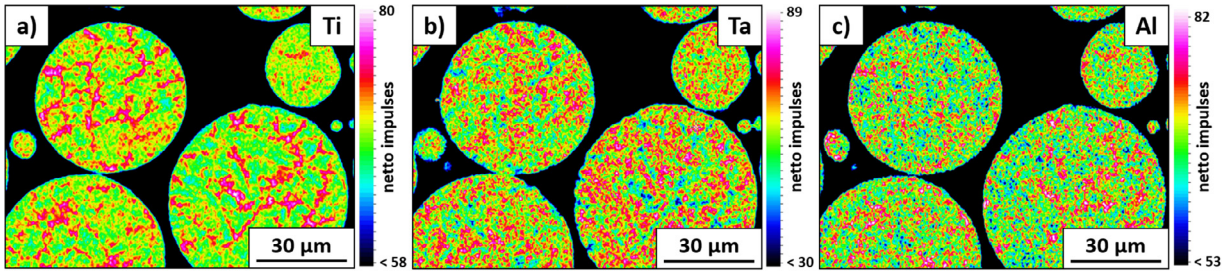

Fig. 2. EDS mappings of pre-alloyed Ti-Ta-Al powder particles showing the element distribution of (a) Ti, (b) Ta, and (c) Al.

machining (EDM). In order to remove the EDM-affected surface layer, the plates were ground down to 5 µm grit size. The additively manufactured Ti-Ta-Al was investigated in two different material states: as-built and after a heat treatment at 1200 °C for 21 h followed by water quenching. All plates were encapsulated in quartz glass tubes under argon atmosphere to avoid oxidation.

For microstructure characterization, plates in both conditions were vibration-polished for 1 h with a 0.04 µm colloidal silica suspension (OP-S NonDry, Struers). Etching was performed for 30 s using Kroll's reagent. Analysis of the process-induced defect distribution was conducted using optical microscopy (OM). For analysis of the chemical composition, local segregations and crystallographic texture, scanning electron microscopy (SEM) including energy-dispersive X-ray spectroscopy (EDS) and electron backscatter diffraction (EBSD) using a Zeiss Ultra Plus Gemini microscope was used. The SEM measurements were performed with an acceleration voltage of 20 – 30 kV. All microsections shown in the following were recorded in a plane parallel to the lateral surfaces, i.e. parallel to the build direction (BD), and depict representative areas from the center of the PBF-EB/M processed cuboids being not affected by surface phenomena.

Phase analysis was carried out at the Deutsches Elektronen-Synchrotron (DESY) at beamline P61A in Hamburg, Germany. High-energy synchrotron diffraction allows to probe sample volumes of several mm^3 and, thus, provides for a detailed high-resolution microstructure analysis. Polychromatic synchrotron radiation, covering an energy range of 20 – 200 keV, and a Mirion high purity Germanium point detector with collimator-slit system were used. For further details on the synchrotron beamline P61A, the reader is referred to Reference [38].

3. Results and discussion

Fig. 1 shows SEM images of the pre-alloyed Ti-Ta-Al powder in as-atomized and sieved condition. Following the EIGA process, the particles are highly spherical and feature smooth surfaces being free of satellites and any defects like cracks. The powder material is fully deagglomerated as seen from the secondary electron (SE) image in Fig. 1a. It should be noted that a slight residual amount of particles with diameters below 25 µm has remained in the sieved powder fraction. However, this fraction has no detrimental effect on the processability (powder flowability and printability) of the powder material at all. Structures with high relative density could be fabricated in this study (cf. Fig. 3 and see details below).

Table 2
Chemical composition determined by EDS of the pre-alloyed Ti-Ta-Al powder and PBF-EB/M processed material in both as-built and annealed condition. For direct comparison, the nominal composition is listed to the top.

	Composition (wt.-%)		
	Ti	Ta	Al
Nominal	70	25	5
Powder	68.3	25.9	5.8
As-built	69.4	25.5	5.1
Annealed	68.0	27.6	4.4

A cross-section backscattered electron (BSE) micrograph of the powder particles is shown in Fig. 1b, indicating a dendritic microstructure. EDS mappings of a polished particle cross-section in Fig. 2 reveal the chemistry of the powder material. Within the limits of EDS accuracy, the quantitative results of the EDS analysis (Table 2) show that the overall chemical composition of the particles is in good agreement with the nominal composition of the Ti-25Ta-5Al alloy. As can be deduced from the mappings, however, the powder particles feature dendrite-type structures, i.e. chemical inhomogeneity associated to microsegregation during solidification. The inter-dendritic phase is enriched in titanium (Fig. 2a). The inherent cooling rates during powder synthesis by EIGA are not sufficiently high to fully prevent segregation processes and, thus, findings are fully in line with results recently reported on gas-atomized Ti-42Nb [36] and tungsten containing Ti-Al powders [39]. Nonetheless, it will be shown below that the PBF-EB/M processed Ti-Ta-Al does not comprise such dendritic microstructural features. Additively manufactured structures with very homogenous element distribution could be obtained using the pre-alloyed powder material for fabrication.

For initial microstructure characterization after PBF-EB/M processing, OM was conducted. A representative micrograph is shown in

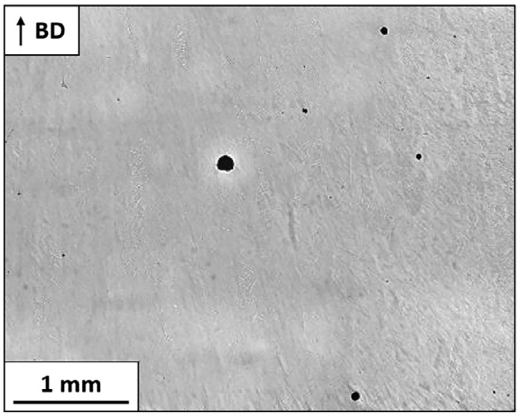

Fig. 3. Optical micrograph depicting the microstructure of PBF-EB/M processed Ti-Ta-Al in the as-built condition. BD is from bottom to top.

Fig. 3 revealing a crack-free microstructure for the Ti-Ta-Al blocks ($10 \times 10 \times 50$ mm^3) in the as-built condition. In AM processes, high residual stresses may result from steep thermal gradients [40,41]. However, elevated base plate and built temperatures effectively reduce process-induced residual stresses [40,41], eventually hampering substantial crack formation as in present case. At this point, size effects are known to have a significant influence on cracking in PBF-LB/M processes, however, PBF-EB/M as a hot-bed AM process does not suffer from such issues to the same extent. Thus, it is expected that the findings discussed and presented here will be transferable to real components. Such assessment, however, is out of the scope of present work and will be the focus of follow-up studies. Only a small contribution of porosity is visible after processing. Using ImageJ software, a relative density of 99.86% has been determined from a series of optical micrographs (not shown). Pore sizes of up to 157 µm (cf. Fig. 3) and an average pore sphericity of 0.96, being very close to a spherical shape, were found. The coincidence of high sphericity and small diameters of pores points at gas porosity induced from gas entrapment in the initial powder material, while the larger pores (cf. defect in the middle of Fig. 3) are likely resulting from keyholing effects [42–44]. Lack of fusion porosity [42], however, has been avoided with the set of processing parameters used in the present work.

In order to shed light on the phase composition of the PBF-EB/M processed Ti-Ta-Al, structure identification was conducted employing high-energy synchrotron diffraction experiments. Fig. 4 shows the corresponding diffraction patterns obtained at room temperature from the additively manufactured material in both as-built and annealed condition. Please note that the latter state will be considered later. The microstructure of the Ti-Ta-Al in as-built condition, i.e. without conducting a post-process heat treatment, mainly consists of the hexagonal close-packed (hcp) α-phase. In addition, minor fractions of the bcc β-phase are also present (cf. the low intensity diffraction peak at around 87.5 keV). The lattice parameters are $a_\alpha = 0.2930$ nm / $c_\alpha = 0.4694$ nm and $a_\beta = 0.3286$ nm for the α- and β-phase, respectively. All parameters are in accordance with data reported in literature for binary Ti-Ta [45,46]. It should be mentioned that no detailed phase diagram is available for the alloy composition investigated. Tantalum and aluminum have opposite influence on the phase formation of titanium alloys; tantalum is a β-stabilizer whereas aluminum is known to stabilize the α-phase [8,45]. Based on the empirical molybdenum equivalency ([Mo]eq) and aluminum equivalency ([Al]eq) [47–49], the Ti-25Ta-5Al alloy can be assessed in the context of β-phase stability, possible constituent phases and resulting microstructure. With a [Mo]eq of 5.5 and an [Al]eq of 5.0, the current Ti-25Ta-5Al alloy, to a large extent, is similar to Ti-6Al-2Sn-4Zr-6Mo (Ti-6246) [47,48,50] as a heat-treatable $\alpha+\beta$ dual-phase alloy. Consequently, the $\alpha+\beta$ dual-phase microstructure observed in PBF-EB/M Ti-25Ta-5Al is supposed to be close to equilibrium state. Due to the relative high processing temperatures of around 850 °C (cf. Section 2) as well as the inherent slow cooling within the process chamber after melting the uppermost layer in PBF-EB/M, decomposition of the high-temperature β-phase into the low-temperature α-phase takes place. In addition, there is no evidence for the existence of the non-equilibrium martensitic phases α' (hcp) and α" (orthorhombic) and the non-equilibrium ω-phase (hexagonal) in the as-built condition (Fig. 4), again indicating near-equilibrium state [45].

The prior-β grain structure as well as the morphology and crystallographic orientation of the volume-dominant α-phase are clarified by the SEM EBSD analysis shown in Fig. 5. The α-phase was indexed with an hcp crystal structure ($P6_3/mmc$) and the lattice parameters determined from the synchrotron diffraction pattern in Fig. 4, i.e. $a_\alpha = 0.2930$ nm / $c_\alpha = 0.4694$ nm. The inverse pole figure (IPF) mapping and the corresponding IPF (Fig. 5b and c, respectively) reveal a well-known Widmanstätten patterned microstructure without an obvious global texture of the α lamellae formed upon PBF-EB/M processing. In bulk metallic materials, microstructures formed during AM, e.g. PBF-EB/M, PBF-LB/M as well as directed energy deposition (DED), are often dominated by columnar grains oriented in BD due to epitaxial growth along the main direction of heat flow [1]. As can be deduced from the SE image (Fig. 5a), the aspect ratios (length/width) of the prior-β grains

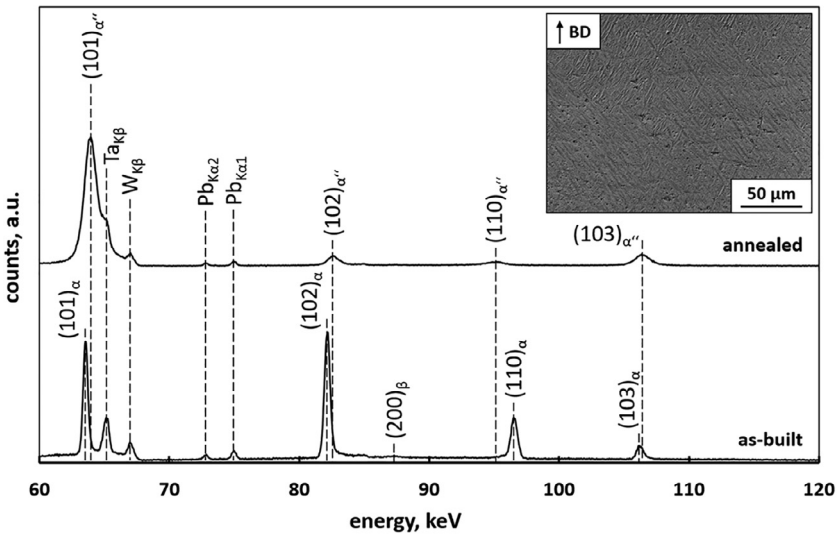

Fig. 4. Synchrotron diffraction patterns of PBF-EB/M processed Ti-Ta-Al in as-built and annealed condition. Additional diffraction peaks of the elements Ta, W and Pb are visible, arising from conventional fluorescence (Ta) and beamline components (W, Pb). Note, the fluorescence peaks of Ti and Al are out of the displayed energy range. The OM image in the inset shows the martensitic microstructure after annealing and etching.

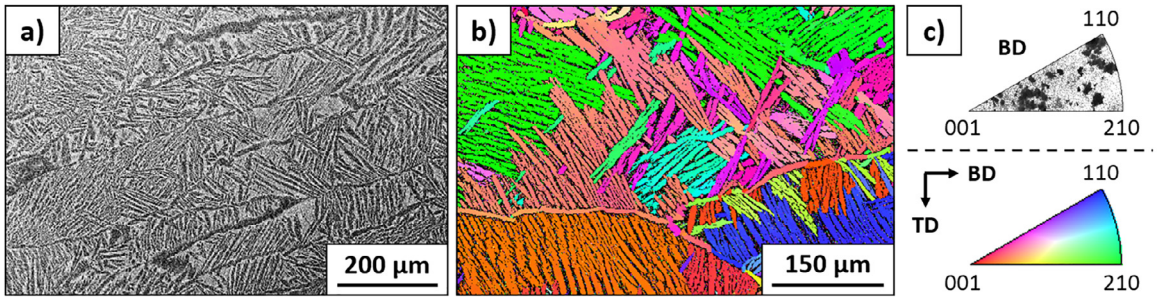

Fig. 5. SEM EBSD analysis of PBF-EB/M processed Ti-Ta-Al in the as-built condition: (a) SE image, (b) IPF mapping, and (c) IPF; (b) and (c) illustrate the crystallographic orientation of the α-phase with respect to BD. The reference coordinate system showing BD in horizontal direction and the color-coded standard triangle for the IPF mapping are shown to the lower right.

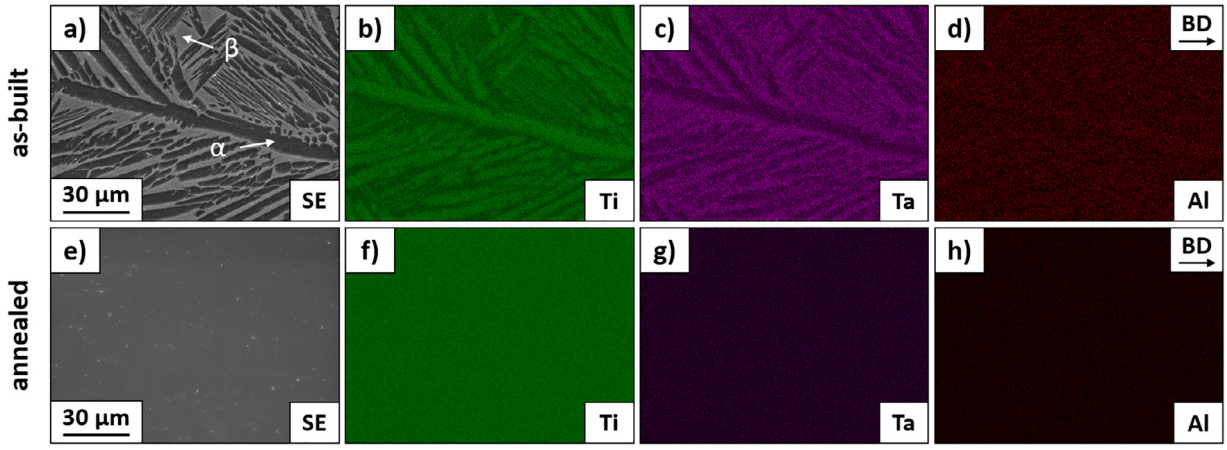

Fig. 6. SEM EDS analysis of PBF-EB/M processed Ti-Ta-Al in the (a-d) as-built and (e-h) annealed condition: (a,e) SE images and (b-d) and (f-h) corresponding EDS mappings. BD is from left to right.

are > 1. Thus, in accordance with grain structures reported in other studies for additively manufactured Ti-Ta alloys [31,51,52], a clear tendency to columnar prior-β grain formation is also visible in the present study. However, it has to be noted that microstructures after PBF-EB/M processing can significantly differ from PBF-LB/M microstructures in terms of the phase composition. The inherent high cooling rates of the PBF-LB/M process effectively hamper diffusion-controlled processes and, thus, *in situ* quenched-in non-equilibrium martensitic phases are often reported in PBF-LB/M fabricated α and α+β Ti alloys [13,31,34,53]. In contrast, (near)-equilibrium phases are typically seen upon PBF-EB/M as rationalized before [13,54].

Upon formation of the α-phase within the parent β-phase by a solid state transformation, the α-phase enriches in α-stabilizer and depletes in β-stabilizer, and vice versa [8]. Beside decomposition, aluminum and tantalum are also known to form intermetallic compounds such as Al_3Ta and $Al_{69}Ta_{39}$ [55,56]. However, the synchrotron results (Fig. 4) provide for clear evidence that these intermetallic phases have not formed in the alloy system under consideration, which is also perfectly in line with detailed microstructure analysis conducted on conventionally processed Ti-Ta-Al alloys in the past [57]. The alloying element partitioning observed in present work is confirmed by EDS results for the Ti-Ta-Al material in the as-built condition (Fig. 6b-d). While in the present study the α-phase (dark areas in Fig. 6a) is enriched in aluminum up to 6.5% (77.7Ti-15.8Ta-6.5Al), a chemical composition of 61.3Ti-34.1Ta-4.6Al with pronounced enrichment in tantalum up to 34.1% is found for the β-phase (bright areas in Fig. 6a). To better assess the overall chemical homogeneity of the PBF-EB/M processed Ti-Ta-Al, a thermal treatment at 1200 °C for 21 h has been conducted. After annealing in the single β-phase region and subsequent water quenching (suppressing diffusion activities effectively), a non-equilibrium, fully martensitic microstructure consisting of the orthorhombic α”-phase evolved as can be seen from the diffractogram and the optical micrograph in Fig. 4. This is akin to the presence of α” martensite in Ti-6Al-2Sn-4Zr-6Mo [48] additively manufactured by PBF-LB/M, where a much higher cooling rate is often achieved compared to PBF-EB/M. The lattice parameters are determined to be $a_{\alpha"} = 0.3083$ nm, $b_{\alpha"} = 0.4948$ nm, and $c_{\alpha"} = 0.4587$ nm. Following both PBF-EB/M processing (as-built condition) and annealing treatment, a slight decrease in the aluminum content can be observed (on the average, global scale) due to evaporation when compared with the initial powder feedstock material (Table 2). However, most importantly the overall element distribution significantly changed upon annealing. As is evident from the EDS mappings in Fig. 6f-h, the initial dendritic microstructure of the powder feedstock material (cf. Fig. 1b and 2) completely vanishes. Accordingly, the constituents, i.e. titanium, tantalum as well as aluminum, are dispersed homogeneously on a submicron scale in the annealed and subsequently quenched condition. In summary, despite obviously tremendous differences in the alloying element densities and melting points, the use of pre-alloyed Ti-Ta based feedstock material, including even low-melting and light elements such as aluminum, allows to overcome current limitations using mixed elemental powders [31,33,34,51,52]. In this regard, the pre-alloyed Ti-Ta-Al powder allows direct fabrication of bulk metallic components featuring microstructures with excellent chemical homogeneity and concomitantly highest density.

4. Conclusions

In the present study, an Al-modified Ti-Ta alloy was successfully additively manufactured by electron beam powder bed fusion (PBF-EB/M) using novel pre-alloyed feedstock material. In order to investigate defect

populations, the chemistry, crystallographic texture, and phase compositions, detailed microstructure analysis was conducted employing optical microscopy (OM), scanning electron microscopy (SEM) including energy-dispersive X-ray spectroscopy (EDS) and electron backscatter diffraction (EBSD), as well as high-energy synchrotron diffraction. The main findings can be summarized as follows:

- Following electrode induction melting inert gas atomization (EIGA), pre-alloyed feedstock material with highly spherical powder particles is obtained. Slight chemical inhomogeneities, i.e. Ta-rich dendritic segregations embedded in a Ti-rich inter-dendritic phase, are found within the particles.
- Ti-Ta-Al bulk structures with densities > 99.86% are fabricated using PBF-EB/M technique. Residual pores are likely resulting from gas entrapments and keyholing effects.
- An $\alpha+\beta$ dual-phase microstructure with columnar prior-β grain structure is observed in the as-built condition. The volume-dominant α-phase is enriched in Ti and Al, featuring a lamellar morphology with no preferred crystallographic orientation.
- After a post-process thermal treatment at 1200 °C for 21 h in argon atmosphere followed by water quenching, a non-equilibrium, fully martensitic microstructure (α''-phase) is present. In this post-processed condition, the Ti-Ta-Al bulk material is characterized by a very homogenous distribution of the alloying elements.

Declaration of Competing Interest

The authors declare that they have no known competing financial interests or personal relationships that could have appeared to influence the work reported in this paper.

Data availability

Data will be made available on request.

Acknowledgments

The authors gratefully acknowledge DESY (Hamburg, Germany), a member of the Helmholtz Association HGF and Helmholtz-Zentrum Hereon, for the provision of experimental facilities. Parts of this research were carried out at PETRA III. Dr. Philipp Krooß and Dr. Guilherme Abreu Faria are thanked for assistance with the experiments and in using P61A – WINE, respectively. Beamtime was allocated for proposal ID: 11012003. C. Lauhoff acknowledges funding by the Alexander von Humboldt Foundation.

References

[1] T. DebRoy, H.L. Wei, J.S. Zuback, T. Mukherjee, J.W. Elmer, J.O. Milewski, A.M. Beese, A. Wilson-Heid, A. De, W. Zhang, Additive manufacturing of metallic components - Process, structure and properties, Prog. Mater Sci. 92 (2018) 112–224, doi:10.1016/j.pmatsci.2017.10.001.

[2] T. Niendorf, F. Brenne, M. Schaper, A. Riemer, S. Leuders, W. Reimche, D. Schwarze, H.J. Maier, Labelling additively manufactured parts by microstructural gradation - advanced copy-proof design, RPJ 22 (2016) 630–635, doi:10.1108/RPJ-12-2014-0183.

[3] C.J. Todaro, M.A. Easton, D. Qiu, D. Zhang, M.J. Bermingham, E.W. Lui, M. Brandt, D.H. StJohn, M. Qian, Grain structure control during metal 3D printing by high-intensity ultrasound, Nat. Commun. 11 (2020) 142, doi:10.1038/s41467-019-13874-z.

[4] M. Froend, V. Ventzke, F. Dorn, N. Kashaev, B. Klusemann, J. Enz, Microstructure by design: an approach of grain refinement and isotropy improvement in multi-layer wire-based laser metal deposition, Mater. Sci. Eng., A 772 (2020) 138635, doi:10.1016/j.msea.2019.138635.

[5] O. Andreau, I. Koutiri, P. Peyre, J.-.D. Penot, N. Saintier, E. Pessard, T. de Terris, C. Dupuy, T. Baudin, Texture control of 316 L parts by modulation of the melt pool morphology in selective laser melting, J. Mater. Process. Technol. 264 (2019) 21–31, doi:10.1016/j.jmatprotec.2018.08.049.

[6] N. Li, S. Huang, G. Zhang, R. Qin, W. Liu, H. Xiong, G. Shi, J. Blackburn, Progress in additive manufacturing on new materials: a review, J. Mater. Sci. Technol. 35 (2019) 242–269, doi:10.1016/j.jmst.2018.09.002.

[7] S. Gorsse, C. Hutchinson, M. Gouné, R. Banerjee, Additive manufacturing of metals: a brief review of the characteristic microstructures and properties of steels, Ti-6Al-4 V and high-entropy alloys, Sci. Technol. Adv. Mater. 18 (2017) 584–610, doi:10.1080/14686996.2017.1361305.

[8] G. Lütjering, J.C. Williams, Titanium, Springer, 2007.

[9] Y.L. Zhou, M. Niinomi, T. Akahori, H. Fukui, H. Toda, Corrosion resistance and biocompatibility of Ti-Ta alloys for biomedical applications, Mater. Sci. Eng., A 398 (2005) 28–36, doi:10.1016/j.msea.2005.03.032.

[10] Y.-.L. Zhou, M. Niinomi, Ti-25Ta alloy with the best mechanical compatibility in Ti-Ta alloys for biomedical applications, Mater. Sci. Eng., C 29 (2009) 1061–1065, doi:10.1016/j.msec.2008.09.012.

[11] E.G. Brodie, K.J. Robinson, E. Sigston, A. Molotnikov, J.E. Frith, Osteogenic potential of additively manufactured TiTa alloys, ACS Appl. Bio Mater 4 (2021) 1003–1014, doi:10.1021/acsabm.0c01450.

[12] P.J.S. Buenconsejo, H.Y. Kim, H. Hosoda, S. Miyazaki, Shape memory behavior of Ti-Ta and its potential as a high-temperature shape memory alloy, Acta Mater 57 (2009) 1068–1077, doi:10.1016/j.actamat.2008.10.041.

[13] S. Liu, Y.C. Shin, Additive manufacturing of Ti6Al4V alloy: a review, Mater. Des. 164 (2019) 107552, doi:10.1016/j.matdes.2018.107552.

[14] W.S.W. Harun, N.S. Manam, M.S.I.N. Kamariah, S. Sharif, A.H. Zulkifly, I. Ahmad, H. Miura, A review of powdered additive manufacturing techniques for Ti-6al-4v biomedical applications, Powder Technol. 331 (2018) 74–97, doi:10.1016/j.powtec.2018.03.010.

[15] A.M. Beese, B.E. Carroll, Review of mechanical properties of Ti-6Al-4 V made by laser-based additive manufacturing using powder feedstock, JOM 68 (2016) 724–734, doi:10.1007/s11837-015-1759-z.

[16] V. Kumar, K.D. Gill, Aluminium neurotoxicity: neurobehavioural and oxidative aspects, Arch. Toxicol. 83 (2009) 965–978, doi:10.1007/s00204-009-0455-6.

[17] D. Zhang, C.S. Wong, C. Wen, Y. Li, Cellular responses of osteoblast-like cells to 17 elemental metals, J. Biomed. Mater. Res. A 105 (2017) 148–158, doi:10.1002/jbm.a.35895.

[18] M. Niinomi, Design and development of metallic biomaterials with biological and mechanical biocompatibility, J. Biomed. Mater. Res. A 107 (2019) 944–954, doi:10.1002/jbm.a.36667.

[19] Y.L. Zhou, M. Niinomi, T. Akahori, Effects of Ta content on Young's modulus and tensile properties of binary Ti-Ta alloys for biomedical applications, Mater. Sci. Eng., A 371 (2004) 283–290, doi:10.1016/j.msea.2003.12.011.

[20] A. Paulsen, H. Dumlu, D. Piorunek, D. Langenkämper, J. Frenzel, G. Eggeler, Laboratory-scale processing and performance assessment of Ti-Ta high-temperature shape memory spring actuators, Shap. Mem. Superelast. 7 (2021) 222–234, doi:10.1007/s40830-021-00334-1.

[21] T. Niendorf, P. Krooß, E. Batyrsina, A. Paulsen, Y. Motemani, A. Ludwig, P. Buenconsejo, J. Frenzel, G. Eggeler, H.J. Maier, Functional and structural fatigue of titanium tantalum high temperature shape memory alloys (HT SMAs), Mater. Sci. Eng., A 620 (2015) 359–366, doi:10.1016/j.msea.2014.10.038.

[22] A. Paulsen, J. Frenzel, D. Langenkämper, R. Rynko, P. Kadletz, L. Grossmann, W.W. Schmahl, C. Somsen, G. Eggeler, A kinetic study on the evolution of martensitic transformation behavior and microstructures in Ti-Ta high-temperature shape-memory alloys during aging, Shap. Mem. Superelasticity 5 (2019) 16–31, doi:10.1007/s40830-018-00200-7.

[23] H.J. Maier, E. Karsten, A. Paulsen, D. Langenkämper, P. Decker, J. Frenzel, C. Somsen, A. Ludwig, G. Eggeler, T. Niendorf, Microstructural evolution and functional fatigue of a Ti-25Ta high-temperature shape memory alloy, J. Mater. Res. 32 (2017) 4287–4295, doi:10.1557/jmr.2017.319.

[24] P.J.S. Buenconsejo, H.Y. Kim, S. Miyazaki, Novel β-TiTaAl alloys with excellent cold workability and a stable high-temperature shape memory effect, Scr. Mater. 64 (2011) 1114–1117, doi:10.1016/j.scriptamat.2011.03.004.

[25] P.J.S. Buenconsejo, H.Y. Kim, S. Miyazaki, Effect of ternary alloying elements on the shape memory behavior of Ti-Ta alloys, Acta Mater 57 (2009) 2509–2515, doi:10.1016/j.actamat.2009.02.007.

[26] H. Sehitoglu, L. Patriarca, Y. Wu, Shape memory strains and temperatures in the extreme, Curr. Opin. Solid State Mater. Sci. 21 (2017) 113–120, doi:10.1016/j.cossms.2016.06.005.

[27] D. Canadinc, W. Trehern, H. Ozcan, C. Hayrettin, O. Karakoc, I. Karaman, F. Sun, Z. Chaudhry, On the deformation response and cyclic stability of Ni50Ti35Hf15 high temperature shape memory alloy wires, Scr. Mater. 135 (2017) 92–96, doi:10.1016/j.scriptamat.2017.03.025.

[28] J. Zhang, R. Rynko, J. Frenzel, C. Somsen, G. Eggeler, Ingot metallurgy and microstructural characterization of Ti-Ta alloys, Int. J. Mater. Res. 105 (2014) 156–167, doi:10.3139/146.111010.

[29] A. Morita, H. Fukui, H. Tadano, S. Hayashi, J. Hasegawa, M. Niinomi, Alloying titanium and tantalum by cold crucible levitation melting (CCLM) furnace, Mater. Sci. Eng., A 280 (2000) 208–213, doi:10.1016/S0921-5093(99)00668-1.

[30] M. Fischer, D. Joguet, G. Robin, L. Peltier, P. Laheurte, In situ elaboration of a binary Ti-26Nb alloy by selective laser melting of elemental titanium and niobium mixed powders, Mater. Sci. Eng., C 62 (2016) 852–859, doi:10.1016/j.msec.2016.02.033.

[31] S. Huang, S.L. Sing, G. de Looze, R. Wilson, W.Y. Yeong, Laser powder bed fusion of titanium-tantalum alloys: compositions and designs for biomedical applications, J. Mech. Behav. Biomed. Mater. 108 (2020) 103775, doi:10.1016/j.jmbbm.2020.103775.

[32] E.G. Brodie, A.E. Medvedev, J.E. Frith, M.S. Dargusch, H.L. Fraser, A. Molotnikov, Remelt processing and microstructure of selective laser melted Ti25Ta, J. Alloys Compd. 820 (2020) 153082, doi:10.1016/j.jallcom.2019.153082.

[33] E.G. Brodie, J. Richter, T. Wegener, A. Molotnikov, T. Niendorf, Influence of a remelt scan strategy on the microstructure and fatigue behaviour of additively manufactured biomedical Ti65Ta efficiently assessed using small scale specimens, Int. J. Fatigue 162 (2022) 106944, doi:10.1016/j.ijfatigue.2022.106944.
[34] E.G. Brodie, J. Richter, T. Wegener, T. Niendorf, A. Molotnikov, Low-cycle fatigue performance of remelted laser powder bed fusion (L-PBF) biomedical Ti25Ta, Mater. Sci. Eng., A 798 (2020) 140228, doi:10.1016/j.msea.2020.140228.
[35] S. Huang, R.L. Narayan, J.H.K. Tan, S.L. Sing, W.Y. Yeong, Resolving the porosity-unmelted inclusion dilemma during in-situ alloying of Ti34Nb via laser powder bed fusion, Acta Mater 204 (2021) 116522, doi:10.1016/j.actamat.2020.116522.
[36] C. Schulze, M. Weinmann, C. Schweigel, O. Keßler, R. Bader, Mechanical properties of a newly additive manufactured implant material based on Ti-42Nb, Materials (Basel) 11 (2018), doi:10.3390/ma11010124.
[37] Markus Weinmann, Holger Brumm, Christoph Schnitter, Melanie Stenzel, Metal powder for 3d-printing(US20220023941A1).
[38] R. Farla, S. Bhat, S. Sonntag, A. Chanyshev, S. Ma, T. Ishii, Z. Liu, A. Néri, N. Nishiyama, G.A. Faria, T. Wroblewski, H. Schulte-Schrepping, W. Drube, O. Seeck, T. Katsura, Extreme conditions research using the large-volume press at the P61B endstation, PETRA III, J. Synchrotron Radiat. 29 (2022) 409–423, doi:10.1107/S1600577522001047.
[39] A. Couret, M. Allen, M.W. Rackel, B. Galy, J.-P. Monchoux, V. Güther, F. Pyczak, P. Sallot, M. Thomas, Chemical heterogeneities in tungsten containing TiAl alloys processed by powder metallurgy, Materialia 18 (2021) 101147, doi:10.1016/j.mtla.2021.101147.
[40] C. Li, Z.Y. Liu, X.Y. Fang, Y.B. Guo, Residual stress in metal additive manufacturing, Procedia CIRP 71 (2018) 348–353, doi:10.1016/j.procir.2018.05.039.
[41] K. Carpenter, A. Tabei, On residual stress development, prevention, and compensation in metal additive manufacturing, Materials (Basel) 13 (2020), doi:10.3390/ma13020255.
[42] M.C. Brennan, J.S. Keist, T.A. Palmer, Defects in metal additive manufacturing processes, J. Mater. Eng. Perform. 30 (2021) 4808–4818, doi:10.1007/s11665-021-05919-6.
[43] G. Chen, Q. Zhou, S.Y. Zhao, J.O. Yin, P. Tan, Z.F. Li, Y. Ge, J. Wang, H.P. Tang, A pore morphological study of gas-atomized Ti-6Al-4 V powders by scanning electron microscopy and synchrotron X-ray computed tomography, Powder Technol 330 (2018) 425–430, doi:10.1016/j.powtec.2018.02.053.
[44] A. Sola, A. Nouri, Microstructural porosity in additive manufacturing: the formation and detection of pores in metal parts fabricated by powder bed fusion, J. Adv. Manuf. Process. (2019) 1, doi:10.1002/amp2.10021.
[45] J.L. Murray, The Ta–Ti (Tantalum-Titanium) system, Bull. Alloy Phase Diagr. 2 (1981) 62–66, doi:10.1007/BF02873705.
[46] A. Ferrari, P.M. Kadletz, T. Chakraborty, K. Liao, D. Langenkämper, Y. Motemani, A. Paulsen, Y. Lysogorskiy, J. Frenzel, J. Rogal, A. Ludwig, C. Somsen, R. Drautz, W.W. Schmahl, Reconciling experimental and theoretical data in the structural analysis of Ti-Ta shape-memory alloys, Shap. Mem. Superelast. 5 (2019) 6–15, doi:10.1007/s40830-018-00201-6.
[47] I. Weiss, S.L. Semiatin, Thermomechanical processing of beta titanium alloys—an overview, Mater. Sci. Eng.: A 243 (1998) 46–65, doi:10.1016/S0921-5093(97)00783-1.
[48] A. Carrozza, A. Aversa, P. Fino, M. Lombardi, A study on the microstructure and mechanical properties of the Ti-6Al-2Sn-4Zr-6Mo alloy produced via Laser Powder Bed Fusion, J. Alloy. Compd. 870 (2021) 159329, doi:10.1016/j.jallcom.2021.159329.
[49] A. Mehjabeen, W. Xu, D. Qiu, M. Qian, Redefining the β-phase stability in Ti-Nb-Zr alloys for alloy design and microstructural prediction, JOM 70 (2018) 2254–2259, doi:10.1007/s11837-018-3010-1.
[50] R. Boyer, G. Welsch, E.W. Collings, Materials Properties handbook: Titanium alloys, ASM International, Ohio, 2007.
[51] S.L. Sing, F.E. Wiria, W.Y. Yeong, Selective laser melting of titanium alloy with 50 wt% tantalum: effect of laser process parameters on part quality, Int. J. Refract. Met. Hard Mater. 77 (2018) 120–127, doi:10.1016/j.ijrmhm.2018.08.006.
[52] L.-.L. Xing, C.-.C. Zhao, H. Chen, Z.-.J. Shen, W. Liu, Microstructure of a Ti-50 wt% Ta alloy produced via laser powder bed fusion, Acta Metall. Sin. 33 (2020) 981–990, doi:10.1007/s40195-020-01052-w.
[53] E.G. Brodie, T. Wegener, J. Richter, A. Medvedev, T. Niendorf, A. Molotnikov, A mechanical comparison of alpha and beta phase biomedical TiTa lattice structures, Mater. Des. 212 (2021) 110220, doi:10.1016/j.matdes.2021.110220.
[54] Y.-.L. Hao, S.-.J. Li, R. Yang, Biomedical titanium alloys and their additive manufacturing, Rare Met. 35 (2016) 661–671, doi:10.1007/s12598-016-0793-5.
[55] H. Okamoto, Al-Ta (Aluminum-Tantalum), J. Phase Equilib. Diffus. 31 (2010) 578–579, doi:10.1007/s11669-010-9786-5.
[56] H. Sina, S. Iyengar, S. Lidin, Reaction behavior and evolution of phases during the sintering of Ta-Al powder mixtures, J. Alloy. Compd. 654 (2016) 103–111, doi:10.1016/j.jallcom.2015.09.100.
[57] T. Niendorf, P. Krooß, C. Somsen, R. Rynko, A. Paulsen, E. Batyrshina, J. Frenzel, G. Eggeler, H.J. Maier, Cyclic degradation of titanium-tantalum high-temperature shape memory alloys — The role of dislocation activity and chemical decomposition, Funct. Mater. Lett. 08 (2015) 1550062, doi:10.1142/S1793604715500629.